Harnessing van der Waals $CrPS_4$ and Surface Oxides for unique pre-set field induced Exchange Bias in Fe_3GeTe_2

Aravind Puthirath Balan[1‡*], Aditya Kumar[1‡], Tanja Scholz[2], Zhongchong Lin[3], Aga Shahee[1†], Shuai Fu[4], Thibaud Denneulin[5], Joseph Vimal Vas[5], András Kovács[5], Rafal E. Dunin-Borkowski[5], Hai I. Wang[4], Jinbo Yang[3], Bettina Lotsch[2], Ulrich Nowak[6], Mathias Kläui[1,7*]

[1]Institute of Physics, Johannes Gutenberg University Mainz, Staudinger Weg 7, 55128 Mainz, Germany.

[2]Max Planck Institute for Solid State Research, Heisenbergstraße 1, 70569 Stuttgart, Germany.

[3]State Key Laboratory for Artificial Microstructure and Mesoscopic Physics, School of Physics, Peking University, Beijing 100871, China.

[4]Max Planck Institute for Polymer Research Mainz, Ackermannweg 10, 55128 Mainz, Germany

[5]Ernst Ruska-Centre for Microscopy and Spectroscopy with Electrons and Peter Grünberg Institute, Forschungszentrum Jülich, 52425 Jülich, Germany

[6]Department of Physics, University of Konstanz, Germany

[7]Centre for Quantum Spintronics, Department of Physics, Norwegian University of Science and Technology, 7491 Trondheim, Norway.

[‡]These authors contributed equally
* Correspondence to aravindputhirath@uni-mainz.de, klaeui@uni-mainz.de

Abstract

Two-dimensional van der Waals (vdW) heterostructures are an attractive platform for studying exchange bias due to their defect free and atomically flat interfaces. Chromium thiophosphate ($CrPS_4$), an antiferromagnetic material, possesses uncompensated magnetic spins in a single layer, rendering it a promising candidate for exploring exchange bias phenomena. Recent findings have highlighted that naturally oxidized vdW ferromagnetic Fe_3GeTe_2 exhibits exchange bias, attributed to the antiferromagnetic coupling of its ultrathin surface oxide layer (O-FGT) with the underlying unoxidized Fe_3GeTe_2. Anomalous Hall measurements are employed to scrutinize the exchange bias within the $CrPS_4$/(O-FGT)/Fe_3GeTe_2 heterostructure. This analysis takes into account the contributions from both the perfectly uncompensated interfacial $CrPS_4$ layer and the interfacial oxide layer. Remarkably, a distinct and non-monotonic exchange bias trend is observed as a function of temperature below 140 K. Interestingly, the occurrence of exchange bias induced by a 'pre-set field' implies that the prevailing phase in the polycrystalline surface oxide is ferrimagnetic Fe_3O_4. Moreover, the exchange bias induced by the ferrimagnetic Fe_3O_4 is significantly modulated by the presence of the van der Waals antiferromagnetic $CrPS_4$ layer, forming a heterostructure, along with additional iron oxide phases within the oxide layer. These findings underscore the intricate and unique nature of exchange bias in van der Waals heterostructures, highlighting their potential for tailored manipulation and control.

KEYWORDS: vdW magnetic materials, exchange bias, vdW heterostructures

Introduction

The phenomenon of exchange bias (EB) arises when a ferromagnetic (FM) material and an antiferromagnetic (AF) material are brought into contact, resulting in the development of a unidirectional magnetic anisotropy at their interface [1]. This introduced anisotropy causes a shift in the magnetic hysteresis loop of the FM along the field axis. EB has significant implications in various device technologies, such as spin valves, which find applications in high-density magnetic storage and sensor systems [2]. The underlying mechanism behind EB is generally attributed to the exchange coupling between uncompensated spins within the AF and the FM moments across the interface [3-4]. However, in thin-film heterostructures comprising non-van der Waals solids, the presence of imperfections like interdiffusion, step edges, grain boundaries, interfacial stress, and roughness can compromise the ideal interface quality [5].

The recent emergence of van der Waals (vdW) magnetic materials exhibiting atomically smooth surfaces has revitalized interest in understanding the microscopic origins of EB [6]. With their inherent layered structure, vdW materials offer the potential to form heterostructures with nearly ideal interfaces, making them particularly promising for investigating interface-related effects, especially pertaining to EB [7]. Recent reports have unveiled the occurrence of EB in vdW FM/AF heterostructures. For instance, an EB of approximately 50 mT was identified in a $CrCl_3/Fe_3GeTe_2$ heterostructure at 2.5 K [8]. Subsequent investigations involved various vdW AF layers ($MnPS_3$, $MnPSe_3$, $FePS_3$) atop metallic Fe_3GeTe_2 or Fe_5GeTe_2 [9, 10]. Remarkably, a substantial EB was observed in a heterostructure composed of a vdW FM insulator and an antiferromagnetic topological insulator ($CrI_3/MnBi_2Te_4$) with partial coverage [11]. Another notable development is the observation of EB in naturally occurring superlattice structures of $MnBi_2Te_4(Bi_2Te_3)n$ ($n = 1, 2$), attributed to exchange coupling between co-existing ferromagnetic and antiferromagnetic constituents in the ground state [12].

Among vdW antiferromagnets, $CrPS_4$ stands out due to its fully uncompensated layered structure, enabling ideal coupling at the interface within vdW FM/AF heterostructures [13-15]. Moreover, Fe_3GeTe_2 (FGT) is an itinerant vdW ferromagnet boasting a substantial Curie temperature of 220 K in bulk [16]. Recent investigations have highlighted that an air-exposed Fe_3GeTe_2 crystal naturally forms a thin antiferromagnetic surface oxide layer (O-FGT), resulting in EB in the underlying unoxidized crystal [17]. Analytical techniques, including energy dispersive spectroscopy mapping, X-ray absorption spectroscopy, and electron energy loss spectroscopy, have indicated a polycrystalline nature for the oxide layer, suggesting the presence of diverse phases such as FeO, Fe_2O_3, and Fe_3O_4 corresponding to varying Fe^{2+} and Fe^{3+} oxidation states [18,19]. This surface oxide has also been found to enhance EB in $CrOCl/Fe_3GeTe_2$ heterostructures [20]. Notably, significant EB has been reported in naturally oxidized and restacked liquid exfoliated Fe_3GeTe_2 nanoflakes [21]. Nevertheless, investigations elucidating the precise magnetic characteristics of the formed oxide layer and its role in introducing EB remain lacking.

This study focuses on the characterization of EB properties within vdW heterostructures, specifically $CrPS_4$/(O-FGT)/Fe_3GeTe_2 and $CrPS_4/Fe_3GeTe_2$, using magneto-transport measurements. Our findings unveil the intricate magnetic signatures underlying the observed robust EB in $CrPS_4$/(O-FGT)/Fe_3GeTe_2, which primarily stems from the dominance of ferrimagnetic magnetite within the surface oxide at the interface. Furthermore, we ascertain that the EB attributed to magnetite is influenced by the presence of vdW $CrPS_4$ in a heterostructure arrangement and the coexistence of a second antiferromagnetic iron oxide phase in the polycrystalline surface oxide. Through a comprehensive analysis of both the complex EB in $CrPS_4$/(O-FGT)/Fe_3GeTe_2 and the intrinsic EB in $CrPS_4/Fe_3GeTe_2$ featuring a pristine interface, this study provides insights into tailoring EB in vdW heterostructures.

Results and Discussions

Single crystals of Fe_3GeTe_2 (FGT) and $CrPS_4$ were grown using chemical vapour transport following previous reports [22], [23]. The quality of synthesized crystals was examined by Raman spectroscopy (please refer to *Figure S1 in Supporting Information Section 1*). All the modes obtained for both Fe_3GeTe_2 and $CrPS_4$ bulk crystals match well with predicted Raman modes [24,25]. To explore the impact of a surface oxide layer (O-FGT) on exchange bias (EB), two heterostructures were created: $CrPS_4$/(O-FGT)/Fe_3GeTe_2 and $CrPS_4$/Fe_3GeTe_2. In the former, a surface oxide layer coats the surface of the Fe_3GeTe_2 flake at the interface, while the latter features a pristine Fe_3GeTe_2 surface. The surface oxide formation was confirmed using element-sensitive cross-sectional transmission electron microscopy measurements (please refer *Supporting Information Section 2* for details) of a $CrPS_4$/(O-FGT)/Fe_3GeTe_2 heterostructure (*Figure S2a-h*). The thickness of the FM and AFM layers of the exposed heterostructure was determined to be 30 nm and 100 nm, respectively, using atomic force microscope (for details please refer to *Figure S3* in *Supporting Information Section 3*). $CrPS_4$/(O-FGT)/Fe_3GeTe_2 heterostructures were fabricated on to a prepatterned anomalous Hall contacts and were subjected to magneto-transport anomalous Hall voltage measurements. Please refer to the methods section for more details about the device fabrication and anomalous Hall voltage measurements. The results obtained are summarised in *Figure 1.* Exchange bias was determined from transport measurements and calculated for each and every measurement as $H_{EB} = \frac{H_C^+ + H_C^-}{2}$, where H_C^+ and H_C^- represent the coercivities at positive and negative fields, respectively.

Initially, we used a magnetic field of +8 T to cool down the $CrPS_4$/(O-FGT)/Fe_3GeTe_2 sample from room temperature to the desired temperatures. Then, we determined the strength of exchange bias (H_{EB}) at these temperatures by analysing the anomalous Hall voltage measured as a function of swept magnetic field. The process was repeated for several

temperature set points from 5 K up to 150 K and the results are summarized in *Figure 1a*. H_{EB} was calculated for all of them and was plotted as a function of temperature (*Figure 1d*). It is generally expected that the magnitude of H_{EB} is maximum at low temperatures and gradually decreases as we go to higher temperatures and disappears above the blocking temperature of the antiferromagnet. However, the H_{EB} here follows a unique and complex non-monotonic trend with the temperature. As indicated by the curve in green circles in *Figure 1d*, the observed trend consists of three distinct regions (indicated by three different colors) characterised by two local minima at ~20 K and ~70 K, respectively. The robust EB observed up to 140 K can be attributed to the surface oxide formation on Fe_3GeTe_2 at the interface as previously reported [17]. However, the complex trend with temperature that we observe has not been studied and reported before. To understand the mechanisms on the low temperature regime, i.e., 5 K to 35 K, one needs to analyse the EB on an h-BN capped $CrPS_4/Fe_3GeTe_2$ device with a pristine interface without any oxide formation (please refer to the *methods* section for details of device fabrication). To analyse the EB of the device with a pristine interface (see *Figure 2c* for the optical image), the device was field-cooled from room temperature to below the Néel temperature of $CrPS_4$ (T_N = 36 K) with an out of the plane field of + 8 T. After the field cooling, AHE measurements were carried out at various temperatures from 5 K to 50 K and are summarised in *Figure 2a*. The H_{EB} calculated was then plotted as a function of temperature (*Figure 2b*). Interestingly, the variation of H_{EB} for a $CrPS_4$/(O-FGT)/Fe_3GeTe_2 was found to be following a similar trend as observed for a pristine $CrPS_4/Fe_3GeTe_2$ interface, however with an enhanced magnitude (*Figure 2d*). The enhancement in the magnitude of H_{EB} observed here is analogous to what has been already observed in CrOCl/(O-FGT)/ Fe_3GeTe_2 heterostructures [20]. The presence of O-FGT layer increases the interface coupling strength between Fe_3GeTe_2 and $CrPS_4$, and further increases the H_{EB} the magnitude of which is found to be greater than the H_{EB} observed for a pristine $CrPS_4/Fe_3GeTe_2$ interface. At 5 K, the magnitude of H_{EB} for a

$CrPS_4/Fe_3GeTe_2$ device with a pristine interface is found to be ~ 12.5 mT ($\pm 5\ mT$) which gradually decreases as the temperature is increased and found to be negligible ($< 2\ mT$) above 20 K which is the blocking temperature of $CrPS_4$. Given the fully uncompensated layer of spins in the $CrPS_4$ at the interface, the comparatively small magnitude of H_{EB} induced by $CrPS_4$ in $CrPS_4/Fe_3GeTe_2$ heterostructure even for 8T field-cooling is counterintuitive and warrants further studies. However, we observed a switching of the polarity of exchange bias from negative to positive at 15 K close to the blocking temperature observed (20 K) which is similar to the observations by S. Ding et al., where they observed similar switching exchange bias behaviour in pristine $CrPS_4$/FeNi interface [22].

Since the H_{EB} of the $CrPS_4$/(O-FGT)/Fe_3GeTe_2 follows a similar trend as that of the h-BN capped $Fe_3GeTe_2/CrPS_4$ device with a pristine interface, the reduced value of $|H_{EB}|$ and sharp decrease to a minimum of about 20 K are then can be attributed to the blocking temperature (T_B) of $CrPS_4$. Moreover, the exchange field of the saturated Fe_3GeTe_2 layer at 20 K may just be sufficient to pin adjacent $CrPS_4$ layer either parallel (ferromagnetic) or antiparallel (antiferromagnetic) to its magnetization direction irrespective of the magnetic ordering of the remaining layers and act as an effective exchange bias [26]. Here, the effective EB seems to be positive and inversely affects the negative EB induced by surface oxide. The influence of this positive EB would be maximum at 20 K corresponding to the minima which reduces gradually and ceases at T_N = 36 K where $CrPS_4$ becomes paramagnetic. This can explain why the $|H_{EB}|$ slightly increases from 20 K to 36 K. Above the $CrPS_4$ Néel temperature of 36 K, only the O-FGT contributes to the EB. The second minimum at 70 K further suggests that two different phases in the surface oxide contribute to EB which is in line with previous reports [18,19]. However, determination of the exact nature of oxide phases is difficult considering the polycrystalline nature of the surface oxide. Here, our investigation of EB in

$CrPS_4$/(O-FGT)/Fe_3GeTe_2 helps us to unravel the nature of two distinct phases of oxides in O-FGT through their unique EB fingerprints.

Surprisingly, unlike the $CrPS_4$/ Fe_3GeTe_2 with a pristine interface, the $CrPS_4$/(O-FGT)/Fe_3GeTe_2 device found to be generating EB even without field-cooling by merely applying a 'pre-set field' (H_{PF}), and the H_{EB} due to ± 1 T pre-set field follows a similar trend as obtained for field-cooling (please see more information about 'pre-set field' in the *methods* section). It is important to note here that the h-BN capped Fe_3GeTe_2/$CrPS_4$ with pristine interface shows exchange-bias only if we do a conventional field-cooling, but remains unbiased for a pre-set field (please refer to *Figure S11* in *Section 11*). Anomalous Hall voltage measurements for h-BN capped $CrPS_4$/(O-FGT)/Fe_3GeTe_2 corresponding to all the three regions for both +1 T and -1 T pre-set fields are summarised in *Figure 1b and 1c*, respectively. H_{EB} was calculated and plotted as a function of temperature (*Figure 1d*, bottom). EB found to be larger for a $\pm$ 1 T pre-set field measurements than those preceded by even an 8 T field cooling at temperatures (for details, please refer to *Figure S4* in *Section 4*) below 20 K, the blocking temperature of $CrPS_4$. This suggests that the dominant phase in the surface oxide layer that contributes to EB could be ferrimagnetic Fe_3O_4 [27, 28]. The dominance of ferrimagnetic Fe_3O_4 in the surface oxide layer is suggested as its magnetic alignment in a particular direction by a pre-set field determines the direction of pinning and hence the direction of loop shift (please refer *Figure S10* in *Supporting Information Section 10*).

Material characterization techniques such as cross-sectional scanning transmission electron microscopy (STEM) – electron energy loss spectroscopy (EELS) and surface sensitive x-ray photoelectron spectroscopy (XPS) (see *Figure S8* and *Figure S9* respectively) are performed to check possible phases of oxides. XPS $2p_{3/2}$ and $2p_{1/2}$ peaks suggest the possible oxide phases are Fe_3O_4, and Fe_2O_3, with both Fe^{3+} and Fe^{2+} valence states. However, the analysis of the Fe-L3/L2 intensity ratio in EELS, in comparison with ratios obtained from

spectra of reference samples, suggests the presence of Fe_3O_4 [19]. The presence of Fe_3O_4 is further supported by the observation of a sudden increase in longitudinal resistance in an O-FGT flake at around 125 K, indicating a Verwey transition in Fe_3O_4 (see *Figure S5a* in *Section 5*).

Importantly, the minimum field required to saturate the ferrimagnetic Fe_3O_4 in the O-FGT at a particular temperature can be considered as the critical pre-set field (H_{CF}) for the system. Therefore, a pre-set field (H_{PF}) greater than the H_{CF} in the preferred direction can be applied to judiciously determine the direction of EB (please refer *Figure S10* in *Supporting Information Section 10*). When the field is swept with a maximum value greater than H_{CF} at a given temperature preceded by a $H_{PF} \geq H_{CF}$, there is no preferred pinning by Ferrimagnetic Fe_3O_4, resulting in zero EB (refer to *Figure S6a-d* in *Section 6*) [27, 28]. In addition to Fe_3O_4, previous reports confirmed the presence of an antiferromagnetic FeO phase in the natural O-FGT [18,19]. This co-existing FeO phase may have a low blocking temperature (T_B) of around 70 K, which is below the bulk Néel temperature (T_N = 198 K) [29]. The FeO phase is responsible for modulating the EB up to 70 K, where we observed a second minimum corresponding to blocking temperature of FeO (refer to *Figure 1d*). Beyond 70 K, the EB is solely due to ferrimagnetic Fe_3O_4, which disappears at 140 K, the identified blocking temperature.

Finally, the complex trend of H_{EB} with respect to the temperature can be understood based on an intuitive model of the contributions of $CrPS_4$ as well as the two iron oxide phases in the O-FGT layer. The intuitive model is schematically represented in *Figure 3*. The various magnetic layers are colour coded. The grey and yellow layers are the bottom and top layers of $CrPS_4$ and Fe_3GeTe_2 on either side of the van der Waals gap, whereas the O-FGT consists of two layers: a thick top layer mainly composed of Fe_3O_4, as suggested by cross-sectional STEM-EELS measurements (see *Figure S8*), and a thin bottom layer composed of FeO, corresponding

to the low valence state of Fe. The presence of two types of oxides layers is also evident from the different contrasts observed in the cross-sectional STEM image of the CrPS4/(O-FGT) Fe_3GeTe_2 interface (*Figure 3a* inset). In the case of the first device with a pristine interface, only a field-cooling below the Néel temperature of $CrPS_4$ (36 K) can induce uniaxial exchange-anisotropy by direct ferromagnetic coupling of $CrPS_4$ moments with Fe_3GeTe_2 moments across the van der Waals gap (*Figure 3a*), whereas, it remains unbiased for a pre-set field (please refer to *Figure S11* in *Section 11*). However, the reason for the observed positive EB close to the blocking temperature is still not understood properly. In the case of the second device with the O-FGT, however, three cases have to be considered: (i) T < 36 K (*Figure 3b*), where all the three constituents are magnetically ordered, (ii) 36 K < T < 70 K (*Figure 3c*), where $CrPS_4$ is paramagnetic, while both oxide phases are magnetically ordered, and (iii) 70 K < T < 140 K (*Figure 3d*), where only Fe_3O_4 is magnetically ordered, and contributes to EB since T_B of FeO is at 70 K. Here, it is important to note that the dominant contribution is due to ferrimagnetic Fe_3O_4 since we are observing a pre-set field induced EB throughout the temperatures from 5 K to 140 K. This is further reinforced by the fact that we already observed no EB due to pristine $CrPS_4$ after a pre-set field. However, here $CrPS_4$ and FeO plays important roles in modulating dominant EB due to Fe_3O_4 in the first two regions where they are magnetically ordered and their contributions to EB is apparent. In the first case, since all the magnetic layers are in their magnetically ordered state, the resulting EB is then the net effect of all three EB contributions. The first local minimum of about ~20 K is identified to be the T_B of $CrPS_4$. It is worth noting that below 20 K, the influence of $CrPS_4$ on H_{EB} is visibly different for field-cooling and pre-set field measurements (*Figure 3c*). H_{EB} is found to be large for 1 T preset-field more than what we obtained for even higher cooling-field of 8 T (please refer *Figure S4* in *Section 4*). This suggests that in addition to modulation, a field-cooled $CrPS_4$ can have converse effects on the magnitude of H_{EB}, whereas $CrPS_4$ under pre-field does not. Magnetic domain level

information is necessary to find out the underlying reason for this contrasting behaviour, which is beyond the scope of this investigation.

Finally, above 70 K, the EB contribution is only from ferrimagnetic Fe_3O_4 that acts directly as the source of pinning, however, through a thin magnetically inactive spacer layer that mainly consists of FeO. This might weaken the longevity exchange coupling, as evident by the significant training effect above 70 K (see *Figure S7* in *Section 7*). Interestingly, we noticed that the strength of the exchange bias caused by Fe_3O_4 is quite high at 80 K, almost as strong as at a much lower temperature of 5 K. This sudden increase in strength above 70 K is reasonable in the sense that the major pinning source is the Fe_3O_4 layer, which acts directly on the Fe_3GeTe_2 without any magnetically active intermediate layers, in contrast to the case where FeO is active below 70 K.

Conclusions

In summary, we have successfully demonstrated exchange bias in $CrPS_4$/(O-FGT)/Fe_3GeTe_2 vdW heterostructures, where we observed a unique and complex non-monotonic trend of exchange bias with temperature. The observed trend is apparent for both field-cooling as well as for a 'pre-set field'. The two local minima observed in the exchange bias trend with the temperature are identified to correspond to the T_B of $CrPS_4$ and FeO. Saturating the ferrimagnetic Fe_3O_4 in the surface oxide by applying a field above a 'critical pre-set field' determines the direction of the unidirectional exchange anisotropy and hence the direction of loop shift, which then allows us to tune the exchange bias. An intuitive model is proposed to explain the complex non-monotonic trend of exchange bias fields as a function of temperature based on the different contributions. Our investigation identifies an alternative approach to tailor exchange bias in van der Waals heterostructures by extrinsic methods such as oxidation combined with applied fields. We believe this investigation will motivate researchers to explore the exceptional tunability of magnetic van der Waals heterostructures for spintronic

applications. Given the large number of AFM vdW materials, our work opens a path to the study of how surface oxide formation on the Fe_3GeTe_2 layer affects the exchange bias when in contact with other vdW antiferromagnets.

References

(1) Blachowicz, T.; Ehrmann, A. Exchange Bias in Thin Films—An Update. *Coatings* **2021**, *11* (2), 122. DOI: https://doi.org/10.3390/coatings11020122

(2) Coehoorn, R. Giant magnetoresistance and magnetic interactions in exchange-biased spin-valves. In *Handbook of Magnetic Materials*, Vol. 15; Elsevier, 2003; pp 1-197.

(3) Schuller, I. K.; Morales, R.; Batlle, X.; Nowak, U.; Güntherodt, G. Role of the antiferromagnetic bulk spins in exchange bias. *Journal of Magnetism and Magnetic Materials* **2016**, *416*, 2-9. DOI: https://doi.org/10.1016/j.jmmm.2016.04.065.

(4) Nogués, J.; Schuller, I. K. Exchange bias. *Journal of Magnetism and Magnetic Materials* **1999**, *192* (2), 203-232. DOI: https://doi.org/10.1016/S0304-8853(98)00266-2.

(5) Fernando, G. W. Chapter 4 - Magnetic Anisotropy in Transition Metal Systems. In *Handbook of Metal Physics*, Fernando, G. W. Ed.; Vol. 4; Elsevier, 2008; pp 89-110.

(6) Gong, C.; Zhang, X. Two-dimensional magnetic crystals and emergent heterostructure devices. *Science* **2019**, *363* (6428), eaav4450. DOI: 10.1126/science.aav4450.

(7) Phan, M.-H.; Kalappattil, V.; Jimenez, V. O.; Thi Hai Pham, Y.; Mudiyanselage, N. W. Y. A. Y.; Detellem, D.; Hung, C.-M.; Chanda, A.; Eggers, T. Exchange bias and interface-related effects in two-dimensional van der Waals magnetic heterostructures: Open questions and perspectives. *Journal of Alloys and Compounds* **2023**, *937*, 168375. DOI: https://doi.org/10.1016/j.jallcom.2022.168375.

(8) Zhu, R.; Zhang, W.; Shen, W.; Wong, P. K. J.; Wang, Q.; Liang, Q.; Tian, Z.; Zhai, Y.; Qiu, C.-w.; Wee, A. T. S. Exchange Bias in van der Waals CrCl3/Fe3GeTe2 Heterostructures. *Nano Letters* **2020**, *20* (7), 5030-5035. DOI: 10.1021/acs.nanolett.0c01149.

(9) Dai, H.; Cheng, H.; Cai, M.; Hao, Q.; Xing, Y.; Chen, H.; Chen, X.; Wang, X.; Han, J.-B. Enhancement of the Coercive Field and Exchange Bias Effect in Fe3GeTe2/MnPX3 (X = S and Se) van der Waals Heterostructures. *ACS Applied Materials & Interfaces* **2021**, *13* (20), 24314-24320. DOI: 10.1021/acsami.1c05265.

(10) Albarakati, S.; Xie, W. Q.; Tan, C.; Zheng, G.; Algarni, M.; Li, J.; Partridge, J.; Spencer, M. J. S.; Farrar, L.; Xiong, Y.; et al. Electric Control of Exchange Bias Effect in FePS3–Fe5GeTe2 van der Waals Heterostructures. *Nano Letters* **2022**, *22* (15), 6166-6172. DOI: 10.1021/acs.nanolett.2c01370.

(11) Ying, Z.; Chen, B.; Li, C.; Wei, B.; Dai, Z.; Guo, F.; Pan, D.; Zhang, H.; Wu, D.; Wang, X.; et al. Large Exchange Bias Effect and Coverage-Dependent Interfacial Coupling in CrI3/MnBi2Te4 van der Waals Heterostructures. *Nano Letters* **2023**, *23* (3), 765-771. DOI: 10.1021/acs.nanolett.2c02882.

(12) Xu, X.; Yang, S.; Wang, H.; Guzman, R.; Gao, Y.; Zhu, Y.; Peng, Y.; Zang, Z.; Xi, M.; Tian, S.; et al. Ferromagnetic-antiferromagnetic coexisting ground state and exchange bias effects in MnBi4Te7 and MnBi6Te10. *Nature Communications* **2022**, *13* (1), 7646. DOI: 10.1038/s41467-022-35184-7.

(13) Bo, X.; Li, F.; Yin, X.; Chen, Y.; Wan, X.; Pu, Y. Magnetic structure and exchange interactions of the van der Waals CrPS 4 monolayer under strain: A first-principles study. *Physical Review B* **2023**, 108(2), 024405.DOI: https://doi.org/10.1103/PhysRevB.108.024405

(14) Calder, S.; Haglund, A. V.; Liu, Y.; Pajerowski, D. M.; Cao, H. B.; Williams, T. J.; Garlea, V. O.; Mandrus, D. Magnetic structure and exchange interactions in the layered semiconductor $CrPS_4$. *Physical Review B* **2020**, 102(2), 024408. DOI: https://doi.org/10.1103/PhysRevB.102.024408

(15) Peng, Y.; Ding, S.; Cheng, M.; Hu, Q.; Yang, J.; Wang, F.; Xue, M.; Liu, Z.; Lin, Z.; Avdeev, M.; Hou, Y.; Yang, W.; Zheng, Y.; Yang, J. Magnetic structure and metamagnetic transitions in the van der Waals antiferromagnet $CrPS_4$. *Advanced Materials* **2020**, 32(28), 2001200. DOI: https://doi.org/10.1002/adma.202001200

(16) Fei, Z.; Huang, B.; Malinowski, P.; Wang, W.; Song, T.; Sanchez, J.; Yao, W.; Xiao, D.; Zhu, X.; May, A. F.; et al. Two-dimensional itinerant ferromagnetism in atomically thin Fe3GeTe2. *Nature Materials* **2018**, *17* (9), 778-782. DOI: 10.1038/s41563-018-0149-7.

(17) Gweon, H. K.; Lee, S. Y.; Kwon, H. Y.; Jeong, J.; Chang, H. J.; Kim, K.-W.; Qiu, Z. Q.; Ryu, H.; Jang, C.; Choi, J. W. Exchange Bias in Weakly Interlayer-Coupled van der Waals Magnet Fe3GeTe2. *Nano Letters* **2021**, *21* (4), 1672-1678. DOI: 10.1021/acs.nanolett.0c04434.

(18) Kim, D. S.; Kee, J. Y.; Lee, J.-E.; Liu, Y.; Kim, Y.; Kim, N.; Hwang, C.; Kim, W.; Petrovic, C.; Lee, D. R.; et al. Surface oxidation in a van der Waals ferromagnet Fe3-xGeTe2. *Current Applied Physics* **2021**, *30*, 40-45. DOI: https://doi.org/10.1016/j.cap.2021.04.022.

(19) Li, Y.; Hu, X.; Fereidouni, A.; Basnet, R.; Pandey, K.; Wen, J.; Liu, Y.; Zheng, H.; Churchill, H. O. H.; Hu, J.; et al. Visualizing the Effect of Oxidation on Magnetic Domain Behavior of Nanoscale Fe3GeTe2 for Applications in Spintronics. *ACS Applied Nano Materials* **2023**, *6* (6), 4390-4397. DOI: 10.1021/acsanm.2c05479.

(20) Zhang, T.; Zhang, Y.; Huang, M.; Li, B.; Sun, Y.; Qu, Z.; Duan, X.; Jiang, C.; Yang, S. Tuning the Exchange Bias Effect in 2D van der Waals Ferro-/Antiferromagnetic Fe3GeTe2/CrOCl Heterostructures. *Advanced Science* **2022**, *9* (11), 2105483. DOI: https://doi.org/10.1002/advs.202105483.

(21) Ma, S.; Li, G.; Li, Z.; Zhang, Y.; Lu, H.; Gao, Z.; Wu, J.; Long, G.; Huang, Y. 2D magnetic semiconductor Fe3GeTe2 with few and single layers with a greatly enhanced intrinsic exchange bias by liquid-phase exfoliation. *ACS Nano* **2022**, 16(11), 19439-19450.DOI: https://doi.org/10.1021/acsnano.2c09143

(22) Ding, S.; Peng, Y.; Xue, M.; Liu, Z.; Liang, Z.; Yang, W.; Sun, Y.; Zhao, J.; Wang, C.; Liu, S.; et al. Magnetic phase diagram of CrPS4 and its exchange interaction in contact with NiFe. *Journal of Physics: Condensed Matter* **2020**, *32* (40), 405804. DOI: 10.1088/1361-648X/ab9e2d.

(23) Och, M.; Martin, M.-B.; Dlubak, B.; Seneor, P.; Mattevi, C. Synthesis of emerging 2D layered magnetic materials. *Nanoscale* **2021**, *13* (4), 2157-2180, 10.1039/D0NR07867K. DOI: 10.1039/D0NR07867K.

(24) Kong, X.; Berlijn, T.; Liang, L. Thickness and Spin Dependence of Raman Modes in Magnetic Layered Fe3GeTe2. *Advanced Electronic Materials* **2021**, *7* (7), 2001159. DOI: https://doi.org/10.1002/aelm.202001159.

(25) Wu, H.; Chen, H. Probing the properties of lattice vibrations and surface electronic states in magnetic semiconductor CrPS4. *RSC Advances* **2019**, *9* (53), 30655-30658, 10.1039/C9RA05861C. DOI: 10.1039/C9RA05861C.

(26) Fu, H.; Liu, C. X.; Yan, B. Exchange bias and quantum anomalous Hall effect in the MnBi2Te4/CrI3 heterostructure. *Science Advances* **2020**, *6* (10), eaaz0948. DOI:10.1126/sciadv.aaz0948

(27) Radu, F.; Abrudan, R.; Radu, I.; Schmitz, D.; Zabel, H. Perpendicular exchange bias in ferrimagnetic spin valves. *Nature Communications* **2012**, *3* (1), 715. DOI: 10.1038/ncomms1728.

(28) Dho, J. Magnetic-field-induced switchable exchange bias in NiFe film on (110) Fe3O4 with a strong uniaxial magnetic anisotropy. *Applied Physics Letters* **2005**, *106* (20), 202405. DOI: https://doi.org/10.1063/1.4921487.

(29) Kozioł-Rachwał, A.; Ślęzak, T.; Nozaki, T.; Yuasa, S.; Korecki, J. Growth and magnetic properties of ultrathin epitaxial FeO films and Fe/FeO bilayers on MgO(001). *Applied Physics Letters* **2016**, *108* (4), 041606. DOI: 10.1063/1.4940890.

FIGURES

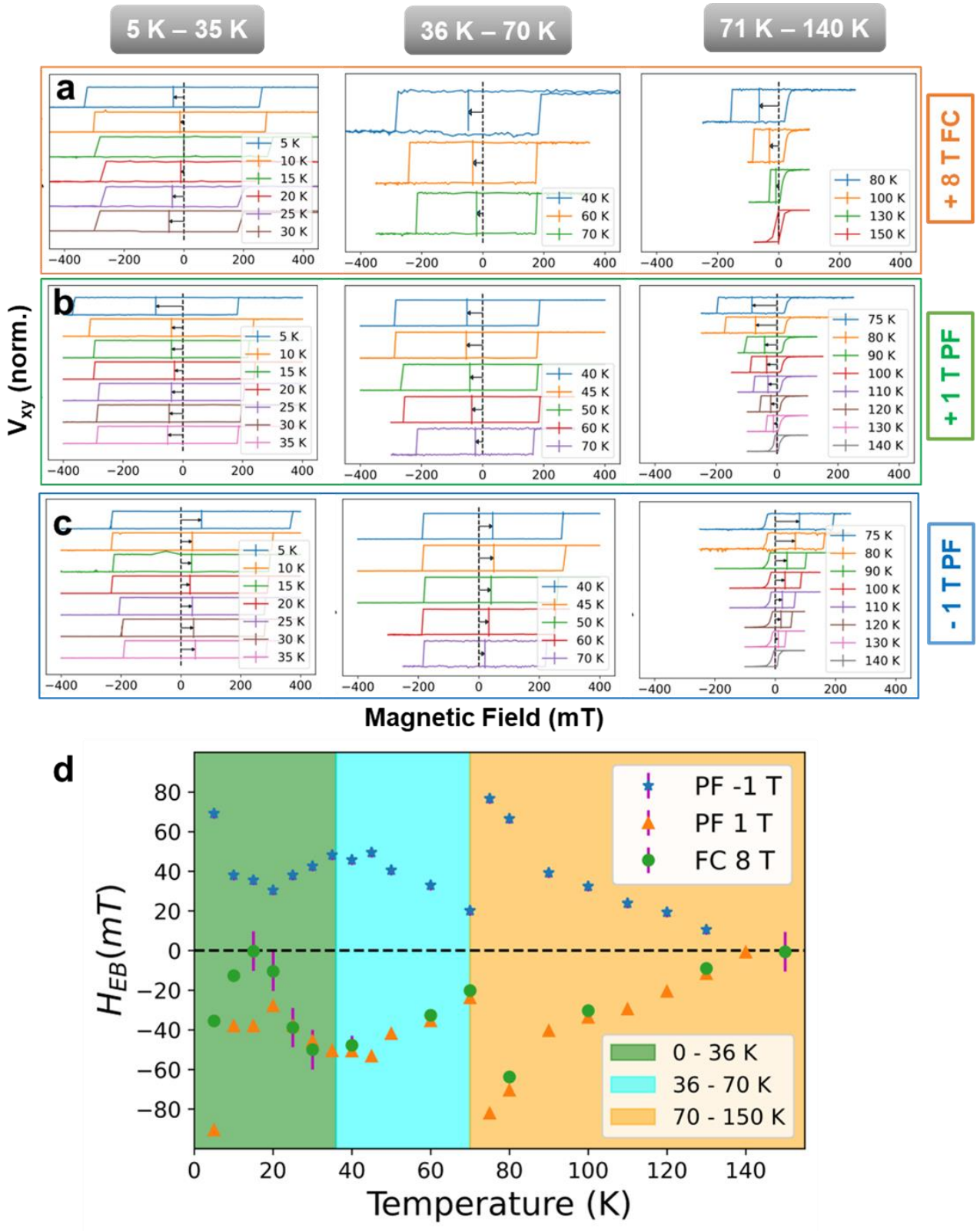

Figure 1. **EB due to surface oxide layers formed at the $CrPS_4$- Fe_3GeTe_2 interface:** EB observed for **(a)** + 8 T field-cooling (FC), **(b)** +1 T pre-set field (PF), **(c)** -1 T pre-set field, and

(d) trend of strength of EB (H_{EB}) as a function of temperature for both +ve (orange) and -ve (blue) 1 T pre-set field experiment as well as for the +8 T field-cooled experiment (green).

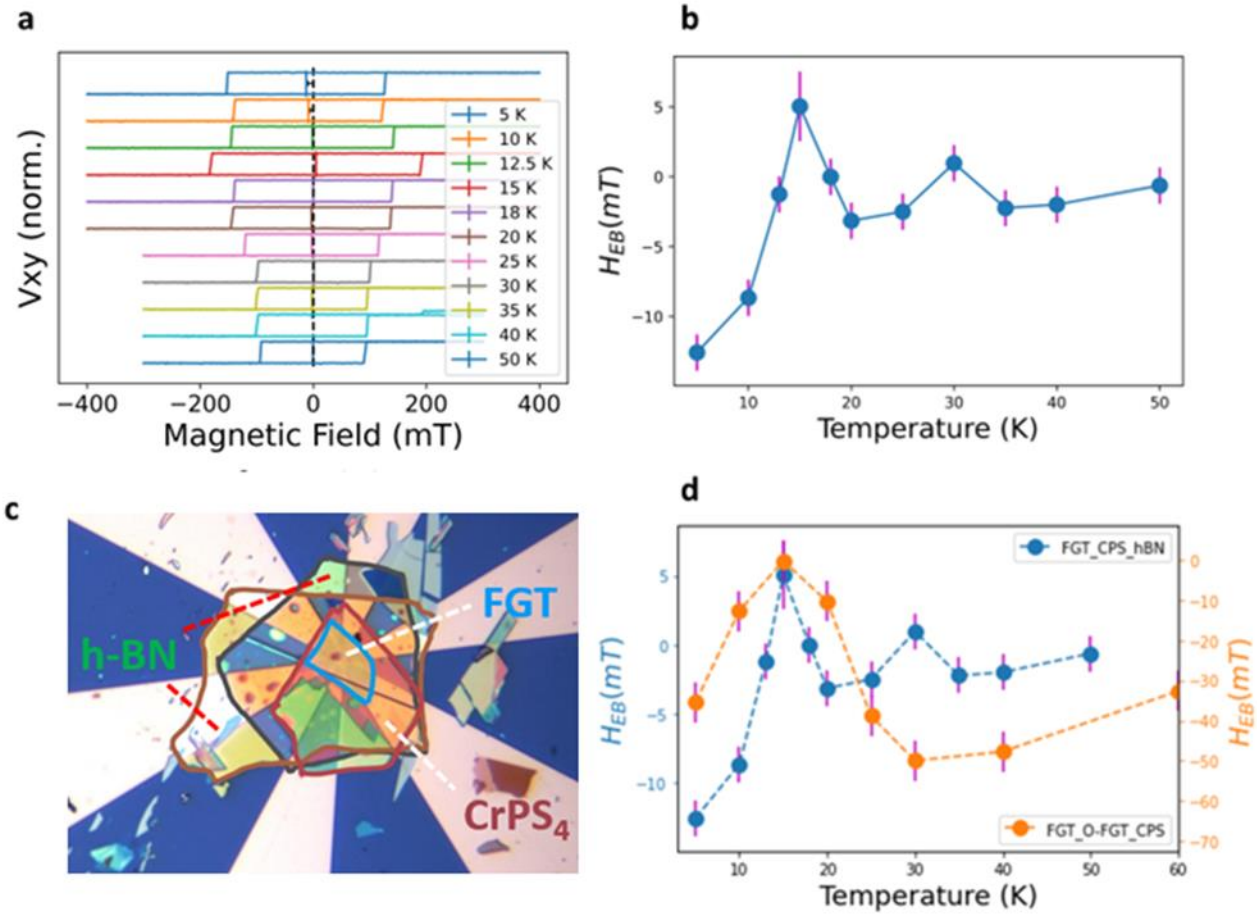

Figure 2. **EB due to a pristine $CrPS_4$/ Fe_3GeTe_2 interface: (a)** EB observed for encapsulated device at various temperatures from 5 K to 50 K for + 8 T field-cooling, **(b)** The trend of strength of EB (H_{EB}) as a function of temperature for + 8 T field-cooling, **(c)** Optical micrograph of hBN/$CrPS_4$/ Fe_3GeTe_2 device (scalebar 10 µm), and (d) Comparison of H_{EB} for a pristine and for an oxygen - exposed devices for + 8T field-cooling.

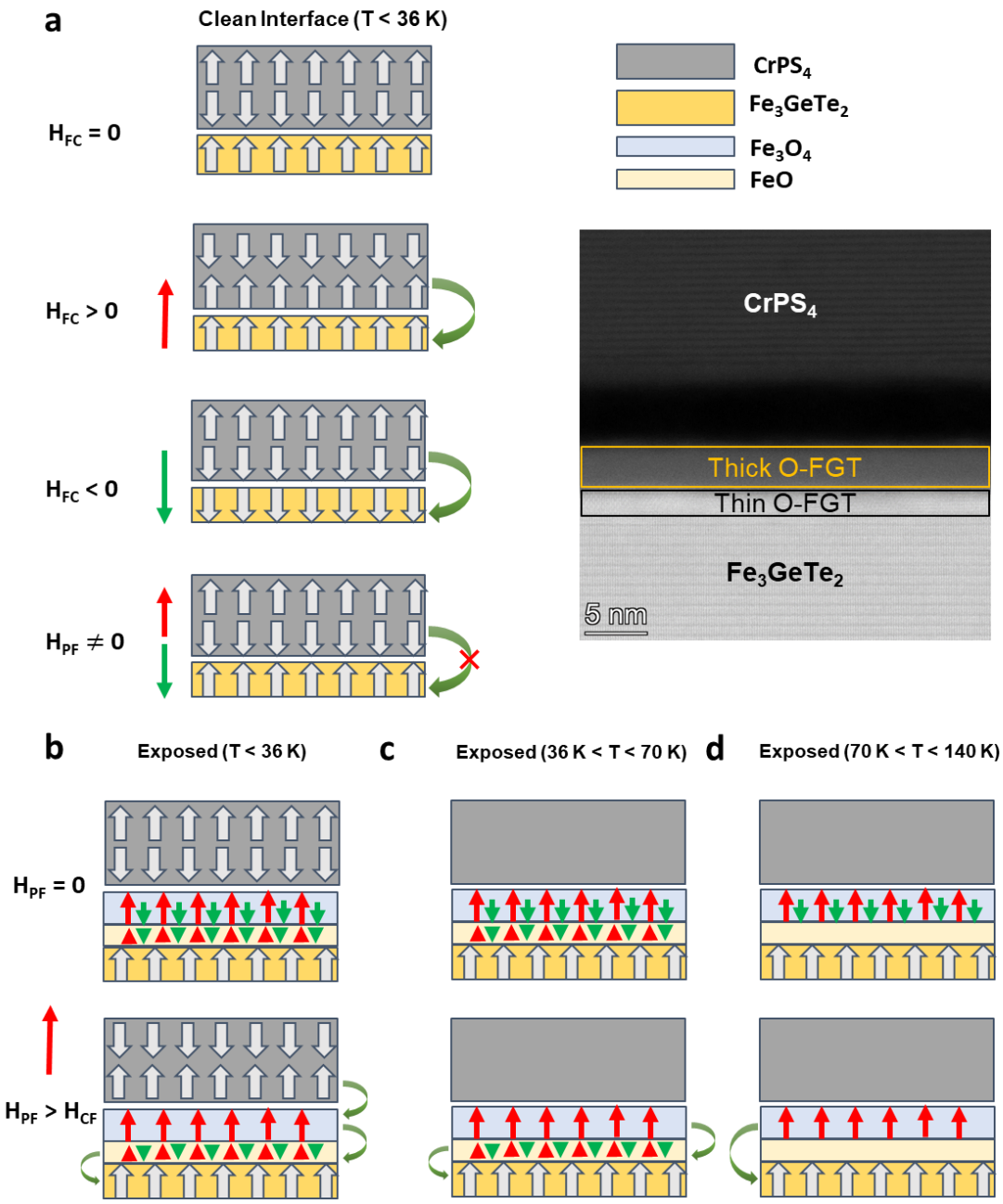

Figure 3. Schematic Model: (a) Exchange coupling in a pristine interface $CrPS_4$/ Fe_3GeTe_2 device after field-cooling (H_{FC}) with the cross-sectional STEM image of the $CrPS_4$/ (O-FGT) Fe_3GeTe_2 in the inset, and the mechanism of exchange coupling induced by a pre-set field (H_{PF}) at different temperature ranges **(b)** T < 36 K **(c)** 36 K < T < 70 K and **(d)** > 70 K. The out-of-plane +ve and -ve field directions are indicated by the long red and green arrows, the exchange coupling is indicated by curved arrows

SYNOPSIS

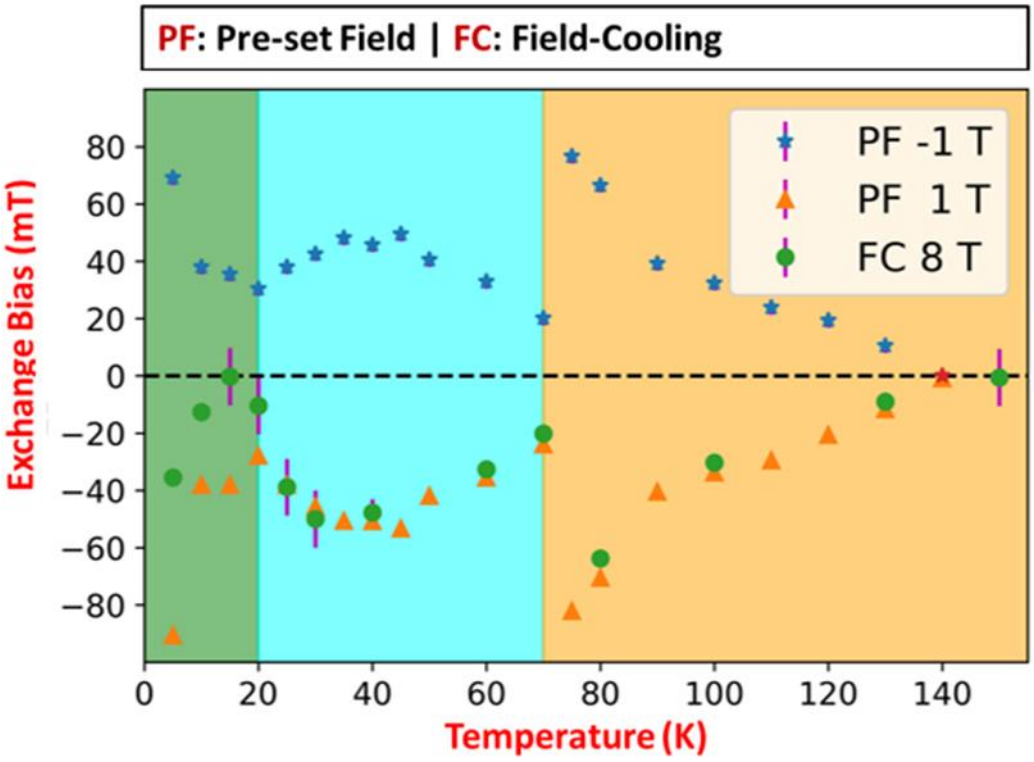

Summary of Research: Unique and non-monotonic trend of the exchange bias as a function of the temperature due to the surface oxide formation on Fe_3GeTe_2 at the interface of the $CrPS_4/Fe_3GeTe_2$ AFM/FM heterostructure

Methods

Few layered flakes of $Fe3GeTe_2$ and $CrPS_4$ were exfoliated onto Si/SiO_2 (300 nm) substrates using standard mechanical exfoliation with scotch tape. The bulk crystals were characterized employing Raman spectroscopy (please refer to *Supporting Information Section 1*). Suitable flakes of uniform thickness were located using an optical microscope. The located FGT and $CrPS_4$ flakes were picked up and transferred in the order mentioned, by typical polymer based dry transfer method, to pre-patterned Hall contacts of Au/Cr (25 nm/5 nm) on Si/SiO_2 (300 nm) fabricated employing standard e-beam lithography. In order to investigate the impact of the surface oxide formed at the FM/AFM interface on EB, the surface of FGT was exposed to an ambient atmosphere for about 30 minutes before transferring the $CrPS_4$ layer resulting in the formation of an ultra-thin oxide layer, which is referred to as (O-FGT). To compare, another $CrPS_4$/ Fe_3GeTe_2 heterostructure with a pristine interface was fabricated the process of which was completely carried out inside the glovebox, containing an inert atmosphere (argon gas), and oxygen and moisture levels were kept below 0.5 ppm, to make sure there is no effect of any oxidation. The fabricated device with a pristine interface was then encapsulated by hexagonal boron nitride (h-BN) flakes to prevent any chances of oxidation in air during sample manipulation. The surface oxide formation was confirmed using element-sensitive cross-sectional transmission electron microscopy measurements (please refer *Supporting Information Section 1* for details) of an exposed FGT flake capped with platinum (Pt) (*Figure S2a-c*). The thickness of the FM and AFM layers of the exposed heterostructure was determined to be $30 \pm 2\ nm$ and $100 \pm 2\ nm$, respectively, using atomic force microscope whereas it was found to be 33.3 ± 11.2 nm and 43.7 ± 9.8 nm for the encapsulated device (please refer to *Figure S1* in *Section 2*). Both devices with a pristine and exposed interfaces were then wire-bonded and immediately loaded onto a variable temperature insert (VTI) cryostat in which we can apply a magnetic field up to 12 T (field precision of ~ 0.1 mT) for

anomalous Hall effect (AHE) measurements. Since $CrPS_4$ is an insulating antiferromagnet, the current will only flow through the metallic FGT layer. The cross-sectional area of the current channel ($10\ \mu m\ x\ 5\ \mu m$) is 1.5 x 10^{-13} $m^{2,}$ and is used to calculate the current density, which is approximately 6.7 x 10^6 Am^{-2} along a 30 nm FGT flake for an applied current of $1\ \mu A$.

A $1\ \mu A$ current was transmitted through the FGT flake along x-direction and the anomalous Hall voltage (V_{xy}) was measured across the transverse terminals along y-direction. The field was applied OOP orientation always for field-cooling, for field sweeping and for application of a *pre-set field**. A Keithley 2400 source meter was used to flow current through the device, and Keithley 2182a nanovoltmeter was used to measure voltage.

**Pre-set Field (Setting Field)*: The pre-set field, which is an out-of-plane field, is the field to which the device was exposed at a specific temperature just before starting the measurement of transverse anomalous Hall voltage (Vxy). It is important to note that the pre-set field and field cooling are different because pre-set field doesn't involve any cooling process through the T_N of the antiferromagnet.

Author Contributions

APB, AK and MK conceive the idea, design and carry out the experiment. TS and BL synthesised the Fe_3GeTe_2 bulk crystals used for the experiments. ZCL and JY synthesised $CrPS_4$ single crystals. SF and HW performed Raman measurements. TD, JVV, AKV and RDB carried out the STEM measurements. AS and UN helped in interpretation of the results. APB, AK contributed equally. All the authors contributed to manuscript writing.

Corresponding Author

Prof. (Dr.) Mathias Kläui
Institute of Physics
Johannes Gutenberg University Mainz
Staudinger Weg 7
55128 Mainz
GERMANY
Email - klaeui@uni-mainz.de

Present Addresses

Dr. Aga Shahee
Ramanujan Fellow,
Centre for Interdisciplinary Research & Innovations (CIRI), University of Kashmir,
Hazratbal, Srinagar-190006 (J&K), India
Email - dr.agashahee@gmail.com

Dr. Shuai Fu
Research Associate, Chair for Molecular Functional Materials
TU Dresden, Walther-Hempel-Bau, Mommsenstraße 4
01069 Dresden, Germany
Email - shuai.fu@tu-dresden.de

Funding Sources

Alexander von Humboldt Foundation for Humboldt Postdoctoral Fellowship (Grant number: Ref 3.5-IND-1216986-HFST-P)

Acknowledgements

We acknowledge funding from the Alexander von Humboldt Foundation for a Humboldt Postdoctoral Fellowship (Grant number: ref 3.5-IND-1216986-HFST-P), EU Marie-Curie Postdoctoral Fellowship ExBiaVdW (Grand Id: 101068014), Deutsche Forschungsgemeinschaft (DFG, German Research Foundation) − Spin + X TRR 173-268565370 (Projects No. A01 and No. B02), DFG Project No. 358671374, Graduate School of Excellence Materials Science in Mainz (MAINZ) GSC 266, the MaHoJeRo (DAAD Spintronics network, Projects No. 57334897 and No. 57524834), the Research Council of Norway (Centre for Quantum Spintronics − QuSpin No. 262633), the National Natural Science Foundation of China (Nos. 12241401 and 11975035), and the European Union's Horizon 2020 Research and Innovation Programme under grant agreement 856538 (project "3D MAGIC"). SF acknowledges the China Scholarship Council for financial support.